Visual Neuroscience (2004), **21**, 611–625. Printed in the USA.

DOI: 10.1017/S0952523804044104

Direction selectivity in a model of the starburst amacrine cell

JOHN J. TUKKER,[1] W. ROWLAND TAYLOR,[2] AND ROBERT G. SMITH[1]

[1]Department of Neuroscience, University of Pennsylvania, Philadelphia
[2]Neurological Sciences Institute, Oregon Health and Science University, Beaverton

(RECEIVED December 15, 2003; ACCEPTED May 12, 2004)

Abstract

The starburst amacrine cell (SBAC), found in all mammalian retinas, is thought to provide the directional inhibitory input recorded in On–Off direction-selective ganglion cells (DSGCs). While voltage recordings from the somas of SBACs have not shown robust direction selectivity (DS), the dendritic tips of these cells display direction-selective calcium signals, even when γ-aminobutyric acid ($GABA_{a,c}$) channels are blocked, implying that inhibition is not necessary to generate DS. This suggested that the distinctive morphology of the SBAC could generate a DS signal at the dendritic tips, where most of its synaptic output is located. To explore this possibility, we constructed a compartmental model incorporating realistic morphological structure, passive membrane properties, and excitatory inputs. We found robust DS at the dendritic tips but not at the soma. Two-spot apparent motion and annulus radial motion produced weak DS, but thin bars produced robust DS. For these stimuli, DS was caused by the interaction of a local synaptic input signal with a temporally delayed "global" signal, that is, an excitatory postsynaptic potential (EPSP) that spread from the activated inputs into the soma and throughout the dendritic tree. In the preferred direction the signals in the dendritic tips coincided, allowing summation, whereas in the null direction the local signal preceded the global signal, preventing summation. Sine-wave grating stimuli produced the greatest amount of DS, especially at high velocities and low spatial frequencies. The sine-wave DS responses could be accounted for by a simple mathematical model, which summed phase-shifted signals from soma and dendritic tip. By testing different artificial morphologies, we discovered DS was relatively independent of the morphological details, but depended on having a sufficient number of inputs at the distal tips and a limited electrotonic isolation. Adding voltage-gated calcium channels to the model showed that their threshold effect can amplify DS in the intracellular calcium signal.

Keywords: Direction selectivity, Starburst amacrine, Morphology, Calcium channels, Modeling

Introduction

Since the discovery of direction selectivity (DS) in the retina (Maturana et al., 1960; Barlow & Hill, 1963), attempts have been made to explain how a direction-selective signal could be computed by the retina's relatively limited circuitry. The focus of these attempts has been on the direction-selective ganglion cells (DSGCs), where DS was first measured. Characteristically, DSGCs generate more spikes in response to a stimulus moving in their preferred direction, and fewer spikes or none in response to stimuli moving in the opposite direction.

Recent evidence suggests that neurons presynaptic to the DSGCs, the starburst amacrine cells (SBACs), may be important for generating DS (Yoshida et al., 2001; Amthor et al., 2002; Euler et al., 2002; Fried et al., 2002). SBACs are found in all vertebrates, have a characteristic radially symmetric morphology (Fig. 1), and tile the inner plexiform layer (IPL) with a coverage factor of 25–70 (Famiglietti, 1983, 1991; Tauchi & Masland, 1984; Vaney, 1984). Bipolar cells make excitatory synaptic contacts throughout the dendritic tree of the SBACs, but outputs from SBACs are limited to the outer third of their dendritic tree (shown red in Fig. 1; see Famiglietti, 1991).

In their recent study, measuring calcium concentration in SBACs, Euler et al. (2002) found weak DS at the soma but robust DS in the dendritic tips. DS in the starburst persisted when $GABA_A$ or $GABA_C$ channels were blocked pharmacologically (Euler et al., 2002; T. Euler, personal communication), indicating that the DS calcium signal does not require inhibition. This result suggested the hypothesis that DS in the starburst cell arises from its distinctive morphology.

As pointed out by Rall (1964), sequential activation of synaptic inputs along a dendrite can generate a signal at the soma that depends on the direction of stimulus motion. At first glance, the radially symmetric morphology of SBACs might seem ill-suited for generating a direction-selective signal; however, it has been postulated that each SBAC dendrite could independently generate a directional signal corresponding to its orientation (Vaney & Young, 1988; Vaney et al., 1989). These directional signals could be preserved in the DSGC if it received inputs only from starburst

Address correspondence and reprint requests to: Robert G. Smith, Department of Neuroscience, Rm 123, Anatomy-Chemistry Bldg., 37th and Service Dr., Philadelphia, PA, 19104-6058, USA. E-mail: rob@retina.anatomy.upenn.edu

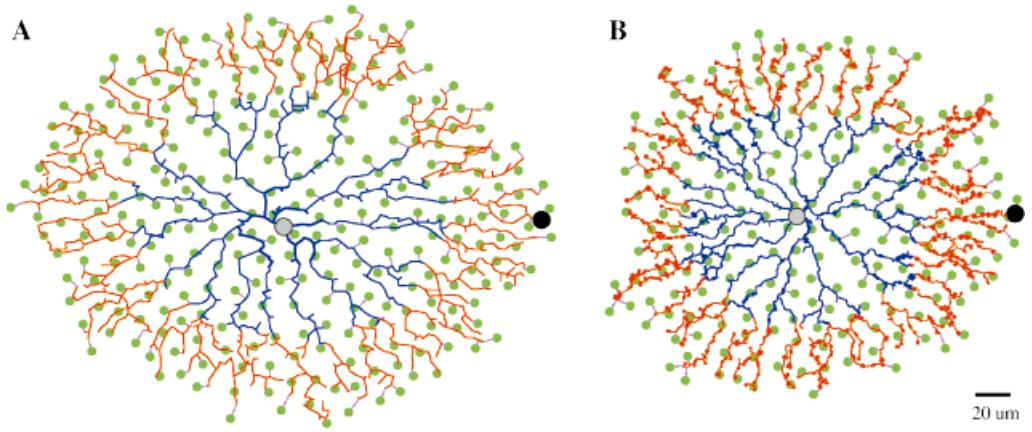

Fig. 1. Starburst morphologies. Shown are soma (gray dot), a dendritic tip recording point (black dot), distal output zone (red), bipolar array (green dots), and synaptic connections to the starburst cell (magenta). A: Cell sb1 (Tauchi & Masland, 1984). B: Cell sbac3 (Taylor & Vaney, unpublished).

dendrites with similar preferred directions (Vaney et al., 1989; Poznanski, 1992; Borg-Graham & Grzywacz, 1992; Fried et al., 2002).

Starburst cells provide direct inhibitory input to the direction-selective ganglion cell (Yoshida et al., 2001; Amthor et al., 2002; Fried et al., 2002), and both excitatory and inhibitory synaptic inputs to the DSGCs are direction selective (Taylor & Vaney, 2002; Fried et al., 2002; S.C. Mangel, personal communication; but see He & Masland, 1997). Since the starburst cell can release both acetylcholine (ACh) and GABA (Brecha et al., 1988; Vaney & Young, 1988; O'Malley & Masland, 1989), it could provide both direction-selective excitation and direction-selective inhibition to different DSGCs.

To investigate the hypothesis that the starburst cell's specific morphological characteristics could generate a direction-selective signal, we constructed compartmental models of starburst cells, added arrays of photoreceptors and bipolar cells to provide synaptic inputs, and measured responses to moving light stimuli. To relate these responses to calcium signals measured in the starburst cell, we determined the effect of calcium channels on the DS signal (red region, Fig. 1).

Materials and methods

Model of starburst cell

Compartmental models were constructed from the digitized morphology of two starburst cells ("sb1", image from Tauchi & Masland, 1984; and "sbac3" from Taylor & Vaney, unpublished). The electrotonic size of the compartments was 0.1 length constant (λ), small enough to preserve most of the spatial detail in a dendritic tree, and commonly used in the literature (Fig. 6B; Rall, 1967; Perkel & Mulloney, 1978; Joyner et al., 1978). For some models, we increased the compartment size to a value (0.65 λ), large enough to reduce the spatial detail in the dendritic tree to the point where several branches of a dendrite were represented by one compartment (Fig. 6B). This was accomplished in the simulator by "condensing" neighboring compartments when their size was larger than a threshold value specified (Smith, 1992, 2004). The simulator preserved the synaptic connectivity and biophysical properties of the membrane during this process so that models run with different compartment sizes could be directly compared.

The starburst cell received excitatory synaptic inputs from a semirandomly spaced array [nearest neighbor distance (NND) of 12 μm, and regularity = 10, see Wässle & Riemann, 1978] of on-bipolar cells, each represented by a single compartment. The semirandom array was generated by an algorithm that added a bipolar cell at a random position but removed it if it did not fit the criteria of the NND and regularity, and repeating this until the cell density was correct (Smith, 2004). Each bipolar cell made one synaptic connection to the nearest SBAC dendrite if it was within a criterion distance (10 μm). The resulting semirandom distribution of synaptic inputs (200–300 per real SBAC morphology) reduced spatial aliasing and was uniform. Although the exact distribution of the starburst's excitatory synaptic inputs is unknown, it is likely to follow the uniform distribution of bipolar cells that provide its synaptic inputs, as is observed in ganglion cells (Freed & Sterling, 1988; Cohen & Sterling 1990; Kier et al., 1995). Each bipolar cell received input from a cone photoreceptor through an inverting synapse. The cone photoreceptors had a flash response corresponding to physiological measurements (Schneeweis & Schnapf, 1999), and included realistic saturation and adaptation functions. Circuitry for creating receptive-field surrounds and extended receptive-field centers in cones and bipolar cells was not included. The synaptic input signal to the starburst cell was a conductance modulated by an exponential function of presynaptic voltage with 2-ms rise and fall times. Although photoreceptors and synapses contained nonlinear transfer functions, for a given intensity and contrast the starburst cell received the same input from every bipolar cell. The value chosen for the synaptic conductance, 110 pS (22 pS unitary conductance, 5 channels per synapse), was plausible but not critical because linear processing was maintained in the starburst by the use of stimuli which did not saturate the synaptic responses.

For most simulations, the starburst membrane properties were passive (axial resistivity, $Ri = 200\ \Omega\cdot$cm, membrane resistivity, $Rm = 50{,}000\ \Omega\cdot\text{cm}^2$, and specific membrane capacitance, $Cm = 1\ \mu\text{F/cm}^2$). Since the properties of the starburst cell in the model were linear, our main conclusions about DS do not depend on the particular values of membrane resistivity, capacitance, synaptic

conductance, or number of synaptic inputs. Although our measurements of some of the time-sensitive parameters, for example, velocity sensitivity, would be expected to vary with the particular values of resistance and capacitance, we did not extensively test the parameter space because this would not affect the main conclusions about DS generated by morphology.

Generating artificial morphology

For some simulations we created an artificial morphology for the starburst cell, allowing us to assess the importance of specific aspects of morphology in generating DS. The diameter of the dendrites varied from 1 μm proximally to 0.5 μm distally, similar to the dendritic taper in real starburst morphology (Tauchi & Masland, 1984). The simplest morphology consisted of a soma with a single branchless dendrite (Fig. 5). More complete models had eight dendrites emanating from the soma, each branching sequentially into subbranches according to a specific rule that depended on the experiment, (Figs. 6A & 6C).

A third type of morphology with a more realistic-looking dendritic tree was created with heuristic rules for branching and mutual self-avoidance (Fig. 10). This morphology started from a soma with five dendritic stubs. The dendrites were incrementally extended a short step (typically 5 μm) within a limited range of directions ($\pm$30 deg) by choosing which direction best avoided nearby dendrites. When the distance from the parent branch-point reached a threshold (typically 25 μm), binary subbranches were created at a preset angle with respect to the parent dendrite (55 deg). This process was repeated, extending the entire dendritic tree one step at a time, until each dendrite either grew nearer than a threshold distance (typically 5–10 μm) to an adjacent dendrite, or extended beyond the preset radius of the dendritic tree. For some models, the preset radius was randomly varied for the different dendrites, creating a range of dendritic lengths (Fig. 10B). For added realism, these models included varicosities (about 3 μm in diameter) at random positions in the outer third of the dendritic tree. The growth increment and thresholds for branching and stopping were varied randomly within a limited range (typically $\pm$20–30%), and beyond 40% radius from soma were modulated as a function of radius from the soma. More details of this algorithm are available in the Neuron-C distribution (Smith, 2004).

According to the connectivity rules of the model, the bipolar cell density and the branching pattern of the starburst dendrites determined the number of bipolar cell connections to the starburst cells. Consequently, a straight dendrite collected few bipolar inputs, a highly branched one collected many, and a "brush-like" pattern of branching near the dendritic tips collected few on the proximal straight portion and many near the tips (Figs. 6A & 6C).

For the simplest model, containing only a soma with a single branchless straight dendrite, responses were averaged over ten models with different random bipolar arrays to minimize spatial aliasing. To reduce the amount of variability in the responses to these different random arrays, we set the density of bipolar inputs slightly higher (nearest-neighbor distance 10 μm instead of the default 12 μm). The effect of this higher number of inputs was offset by decreasing the stimulus and background intensity levels.

Calcium channels

For some simulations, we explored the effect of voltage changes on transmitter release by including Q-type calcium channels (Jensen, 1995; Cohen, 2001) in the synaptic output zones (delineated in Fig. 1). To simplify interpretation of this series of simulations, we set the calcium conductance density to a low enough value (50 μS/cm^2) that the calcium current had a negligible effect on the membrane voltage. The calcium channel was defined as a discrete-state Markov scheme similar to Serrano et al. (1999), except that it had eight states, and two activation and two inactivation rate functions (Fig. 2A). We adjusted the voltage offsets and the multiplier constants for the rate functions to approximately match the behavior of Q-type channels described in Sather et al. (1993).

The rate constants were calculated at a given potential according to the equations:

$$a = 18570 * \frac{-0.09 * (V - 67)}{\exp[-0.09 * (V - 67)] - 1},$$

$$b = 10 * \exp[(V - 32)/-25],$$

$$c = 0.36 * \exp[(V + 16)/-9],$$

$$d = 0.867 * \frac{-0.05 * (V + 16)}{\exp[-0.05 * (V + 16)] - 1},$$

where the units for a, b, c, d were s^{-1}, and the units for V were mV. The Q-type channels defined by the model activated strongly at voltages more depolarized than $-$40 mV (Fig. 2B), and at $-$30 mV had a slowly inactivating component with a time constant of $\sim$150 ms. Along with the calcium channels we included radial calcium diffusion in shells and a calcium pump sufficient to reduce $[Ca^{2+}]_i$ within a short time constant (van Rossum et al., 2003).

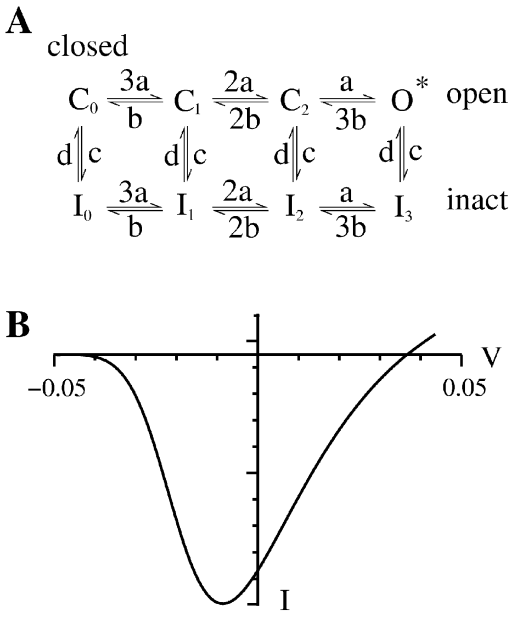

Fig. 2. Properties of calcium channels used in simulations. A: Markov diagram showing the eight discrete states of each channel, including the weighted activation (a,b) and inactivation (c,d) rate functions. O*, open state; $C_{0\text{-}2}$, closed states; $I_{0\text{-}3}$, inactivated states. B: Current–voltage relation of peak calcium currents (after Sather et al., 1993). Channel opens when membrane potential depolarizes beyond $-$40 mV. I: normalized current.

Stimuli

Stimuli comprised bars, spots, annuli, sine-wave gratings, or concentric sine waves moving over the cell in opposite directions. Edges (e.g. very wide bars) were not presented because the model lacked the spatial antagonism necessary to generate response peaks from an edge. The bar stimulus, with long axis extending beyond the cell and perpendicular to its motion, moved from outside of the starburst's dendritic tree to and fro over the entire cell. The annulus contracted from slightly beyond the radius of the starburst dendritic tree down to 20% of the radius, and then expanded again. Spot stimuli consisted of two round spots presented sequentially, the first over the dendritic tip, and the second at an adjacent more proximal location. The opposite direction was created by reversing the order. The apparent motion velocity was adjusted by manipulating the duration of the flashes and the time intervals between them. Although we tested various stimulus sizes, for the results presented here the width of all bars, annuli, and spots was 30 μm unless otherwise noted. Drifting sine-wave stimuli covered the entire cell, with spatial frequencies ranging from 0.5 cycles to 3 cycles per dendritic radius in steps of 0.1 (normalized per dendrite). Gratings were oriented perpendicular to their axis of motion. Concentric sine waves were centered on the soma, with either expanding or contracting motion, and in some experiments also had a round mask at mean intensity (Euler et al., 2002), centered over the starburst soma, with a radius equal to 30% of the dendritic tree radius. After confirming in initial simulations that the DS for the linear model was largely independent of contrast, we set the sine-wave contrast to 80%.

Stimulus motion for most simulations was parallel to the dendrite being recorded from, that is, radial, except when we tested for dendritic orientation preference. Thus we will refer to centrifugal motion if the stimulus moves outwards towards the dendritic tips, and centripetal motion if the stimulus moves towards the soma. For all stimuli, we measured the responses to radial motion at 16 different dendritic tips around the dendritic tree, which produced different amounts of DS depending on the particular dendritic tip. For bar, spot, and annulus stimuli, the DS we report was from the dendritic tip that produced the maximal DS response (see Fig. 5), whereas for sinusoidal stimuli we report the average DS to smooth contours in the two-dimensional (2D) plots (Fig. 9).

Velocities for sinusoidal stimuli ranged from 100 μm/s to $\sim$4000 μm/s at intervals of a factor of 1.5, while for nonsinusoidal stimuli the maximal velocity was $\sim$10,000 μm/s. Stimulus and background intensity were varied for the different simulations to maintain the starburst model membrane voltage within a range of -35 to -58 mV. Before every simulation, the photoreceptor units were exposed to the background light level until they reached a steady state (typically $\sim$500 ms). Optical blur and photon noise were not included in these simulations. The entire model, including light stimuli, arrays of photoreceptors and bipolar cells, starburst cell, synaptic connections, and calcium channels, was implemented in the simulation language Neuron-C (Smith, 1992, 2004).

Measurement of responses

To measure how the wave-shape varied with distance from soma, voltage responses were recorded at four roughly equidistant points along a dendrite. Since the intermediate points gave intermediate responses, we report here only voltages at the soma and dendritic tips.

We determined input resistance, $R_{in} = dV/dI$, by measuring the steady-state current in response to a voltage step (from -50 mV to -30 mV) for several different amounts of synaptic input.

The starburst model produced a linear response to light stimuli and therefore different stimulus directions evoked responses with identical time integrals. However, the wave-shapes differed depending on the stimulus direction, implying that with a suitable nonlinearity the amacrine cell could provide a DS signal for the ganglion cell. Therefore, we computed DS signals based on the difference in peak amplitudes that resulted from the directional differences in the response wave-shapes (Borg-Graham & Grzywacz, 1992).

We quantified starburst DS by calculating a DS index, denoted *DSI*:

$$DSI = (Vcf - Vcp)/(Vcf + Vcp),$$

where "*Vcf*" and "*Vcp*" are the peak evoked responses (normally measured at the dendritic tip) in the centrifugal and centripetal directions, respectively. A *DSI* of 0 indicates no DS, 1 indicates maximal DS with the preferred direction being centrifugal, and -1 indicates maximal DS with a centripetal preference. Although the *DSI* does not necessarily reflect the physiological significance of the response, it allows comparison between responses of different magnitude. For simulations with stimuli containing drifting sine waves, a similar DS index was computed based on the peak-to-peak voltages of the sinusoidal response. For very high temporal frequencies, where the voltage response was small and hence its accuracy was limited, we report only those responses where the peak-to-peak voltage was greater than a criterion value (0.1 mV) for both directions of stimulus motion.

Results

Input resistance

To understand the effect of the starburst morphology on EPSP amplitude, we computed the input resistance R_{in} at several points on each dendrite and at different levels of synaptic activation (see Methods). As expected, R_{in} was lower at proximal than at distal points (Fig. 3), consistent with the known effects of the axial and membrane resistances and dendritic diameter on input resistance [$R_{in} \sim \sqrt{(Ri * Rm/d^3)}$, Rall, 1959]. R_{in} for proximal dendrites was reduced by their thicker diameter and the proximity of the current sink represented by the soma with its attached dendrites. Removal of all but one of the dendrites ("single den" in Fig. 3) reduced the soma's load, making proximal R_{in} higher. R_{in} is highest at the dendritic tip because there (the farthest point from the soma) total axial resistance is highest and because only one path exists for current to flow away from a local stimulus. The greater R_{in} at distal dendritic tips increased their response to local synaptic input. However, when the background light intensity level was increased,the additional synaptic activation from bipolar cells reduced R_{in} (Fig. 3), thereby reducing λ and the spread of signals (Velte & Miller, 1997).

Simulations using bar stimuli

When we passed a bar stimulus in both directions over the entire cell and recorded the response at a dendritic tip, the peak response in the centrifugal direction was greater than in the centripetal direction, with a *DSI* of $\sim$0.2 (Fig. 4). This showed that, in the

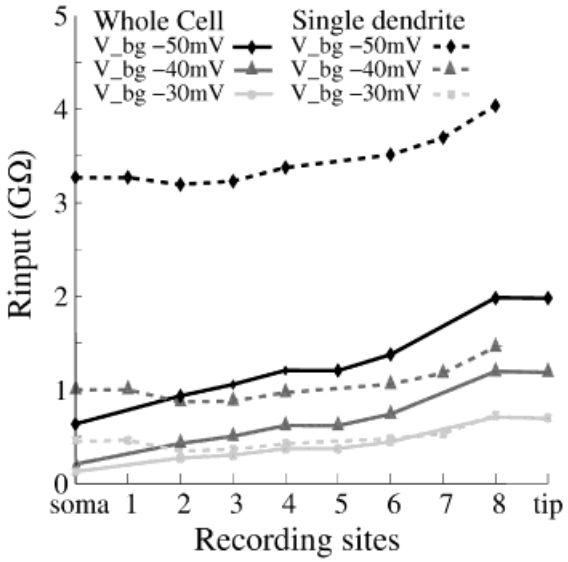

Fig. 3. Input resistance R_{in} increases with distance from the soma. For both the whole cell (straight lines) and a soma with just one dendrite (dashed lines), measurements were taken at sites along the length of the dendrite. R_{in} varies inversely with the bipolar cells' background depolarization (V_bg), measured at three values, −50 mV (subthreshold, g/synapse = 0 pS), −40 mV (∼half activation, g/synapse = ∼50 pS), and −30 mV (saturated, g/synapse = 110 pS). Cell sb1.

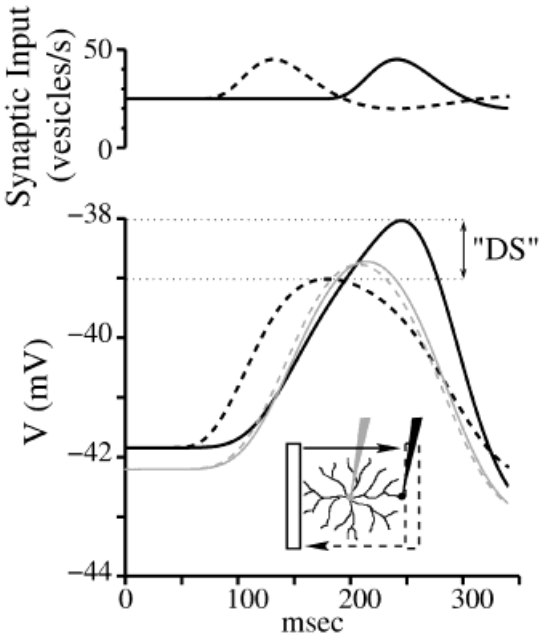

Fig. 4. Morphology-based model generates DS. Top panel: Synaptic input at the dendritic tip for centrifugal motion (continuous) and centripetal motion (dashed). Bottom panel: Voltage responses at dendritic tip (dark trace) and soma (light trace). At the dendritic tip, a moving bar stimulus elicited a greater peak response for centrifugal motion (continuous trace) than for centripetal motion (dashed trace). This difference represents DS (*DSI* ∼ 0.2). The response at the soma was nearly identical for both directions (*DSI* ∼0). Baseline membrane potential was more depolarized at the dendritic tip because of a larger R_{in} and more synaptic connections. Cell sb1, results were similar for sbac3. Velocity = 2000 μm/s.

absence of active mechanisms, the cell's morphology could generate DS.

As the stimulus bar moved across the cell towards the soma, the number of activated synapses gradually increased, reaching a broad maximum when the bar approached the soma. From each activated synapse, current spread to the soma, forming a "global" EPSP that spread throughout the dendritic tree. As the bar passed beyond the soma towards the recording site at the dendritic tip, the EPSPs generated locally within the dendrite superimposed on the continuing global EPSP, so that the local and global EPSPs summed, producing a large peak response in the centrifugal ("Preferred") direction. For the opposite direction, the stimulus activated the local inputs in the dendritic tips before the global EPSP became established. In this case, the local and global EPSPs did not coincide, producing a smaller peak response in the centripetal ("Null") direction. A recording from the soma showed equal responses in both directions, giving no DS, and indicating that the measured DS depended upon an asymmetry of the recording location relative to the stimulus.

To explore how DS depended on the amount of spatio-temporal summation of global signals, we carried out a number of simulations with the same bar stimulus but with different velocities and SBAC morphologies. Measuring DS in models with real morphologies (see Fig. 1), we found that although directional responses at the dendritic tips showed considerable variability (±50%), they all displayed clear velocity tuning (Fig. 5A). Variability of DS for other morphologies and types of stimuli was similar (not illustrated). To study how locally the DS-generating mechanism might function, we performed the same experiment using morphologies that contained only a soma and the dendrite being recorded from. Reducing the morphology even further, we presented the same stimulus to a model with only a soma and one straight branchless dendrite.

The highest *DSI* occurred with bars moving at relatively high velocity over the whole cell (Fig. 5B). DS generated by a cell with just one dendrite (*DSI* 0.03–0.08) was less, suggesting that other dendrites, while having different preferred directions, still contribute to generating DS. Straight branchless dendrites generated only weak DS (Fig. 5B). These results indicated that some feature specific to branched morphology is important for generating DS.

In simulations with bars of different widths (20–150 μm), we found that wider bars gave lower *DSI* values, indicating that DS can be generated more efficiently from thinner stimuli (not illustrated). Although wider bars gave greater response amplitudes, they covered a larger part of the dendrite, reducing DS by mixing the global and the local signals.

Simulations using spots and annuli

To explore how DS depended on interaction of local and global signals, we computed the *DSI* for spots and annuli, and compared them to the *DSI* for bars (Fig. 5C). The cells' response to an expanding and contracting annulus showed very little direction selectivity (*DSI* ∼ 0.04, Fig. 5C). Since the annulus was symmetric with respect to the SBAC morphology, the EPSPs it generated in all dendrites were synchronous, reducing current flow between them and limiting the summation of local and global signals. Two sequentially presented spots also generated a lower peak *DSI* than for the bar stimulus (*DSI* ∼0.09), and showed a preference for lower velocities (Fig. 5C). The reason was that the two-spot

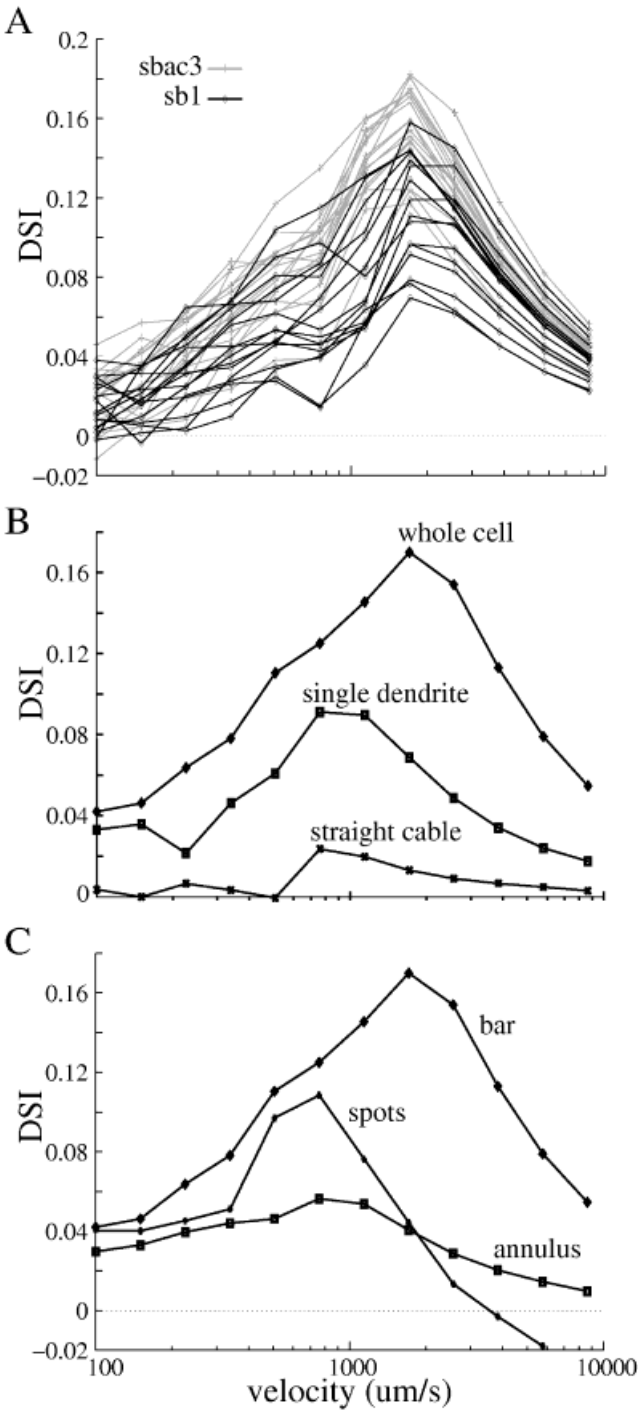

Fig. 5. DS measured at dendritic tips is robust and shows velocity tuning. A: DS responses of two model cells, measured at 16 dendritic tips for radially moving bars. Responses within a cell differ up to ± 50% but all show robust DS and velocity tuning. B: Moving bars gave greatest *DSI* in a whole cell (see Fig. 1). When all but a single dendrite were removed, DS was attenuated. For a soma and dendrite lacking side branches ("straight cable"), DS was nearly abolished. Points depict the average of the maximal *DSI* from both cells, each determined from 16 different dendritic tips as described in *Methods*. Maximal *DSI* was similar for both cells. C: DS responses for two-spot and annulus are attenuated compared to bar stimulus. As in B, points depict the average of both cells' maximal DS responses. Stimulus width = 30 μm.

stimulus moved a smaller distance than the bar and covered less of the dendritic tree, so the cell could not sum signals from as large a region.

Morphology

To explore what properties of the cell were important in shaping its responses, we generated artificial morphologies that shared the basic features of the real cells, but which could be easily manipulated quantitatively.

Since we had already determined that a dendritic tree without branching did not produce much DS, we next considered what effect the specific branching pattern might have. Simplifying the artificial morphology using straight cable segments, we tested different combinations of soma diameter, dendritic diameter, axial resistance, dendritic tree radius, and branching pattern (see *Methods*). In each model, variability in the number of synaptic inputs onto the artificially generated starburst dendrites originated from the semirandom array of bipolar cells, which made synaptic connections according to their proximity to a starburst dendrite (see *Methods*).

When we varied the distance to the first branch-point while preserving the locations of the dendritic tips, DS was relatively unaffected (Fig. 6A). However, when the first branch-point was within 20 μm of the tips, we did not include all the branch-points, reducing the number of synaptic inputs at the dendritic tips. For this extreme "brush-like" morphology, DS was reduced (Fig. 6A), suggesting that the number of distal synaptic inputs is more important than the precise pattern of branching.

To further explore the importance of the branching pattern, we increased the compartment size for the simulator, which reduced the level of morphological detail in the model (Fig. 6B, see Methods). This manipulation changed the effective morphology of the starburst cell while preserving its input pattern. An increase in compartment size did not affect the amount of DS generated, provided that there was a symmetric arrangement of dendritic compartments around a central compartment (soma).

The relative insensitivity of DS to the exact pattern of dendritic branching suggested that the spatial distribution of synaptic inputs might be important for DS. With the parsimonious assumption of a uniform array of inputs, a starburst dendrite covering a wedge-shaped area receives most inputs near the dendritic tips (see Methods), suggesting that this effect of morphology might be important for DS. To explore this effect, we constructed models with a first branch-point located distally, and increased the amount of branching beyond that point. We found that the *DSI* was proportional to the number of branch-points (Fig. 6C), suggesting that the amount of membrane surface area and/or number of inputs in the distal zone is important for generating DS. When we increased the synaptic strength and/or the number of synapses in the distal zone of the zero branch-point model, without any explicit change in the electrotonic properties, its *DSI* increased up to two-fold (not illustrated).

If DS does not depend on the details of dendritic branching but upon the spatial location of inputs, then the electrotonic coupling from the dendritic tips to the soma must be important for generating DS signals. To assess how the electrotonic properties contribute to DS, we varied the axial membrane resistivity *Ri*, and tested for DS with a bar stimulus and the same "brush-like" morphology (Fig. 6C, 3 branch-points). The maximum *DSI* was observed for an intermediate *Ri*, corresponding to a λ of 400 μm (Fig. 7), not much larger than the dendritic spread of the starburst

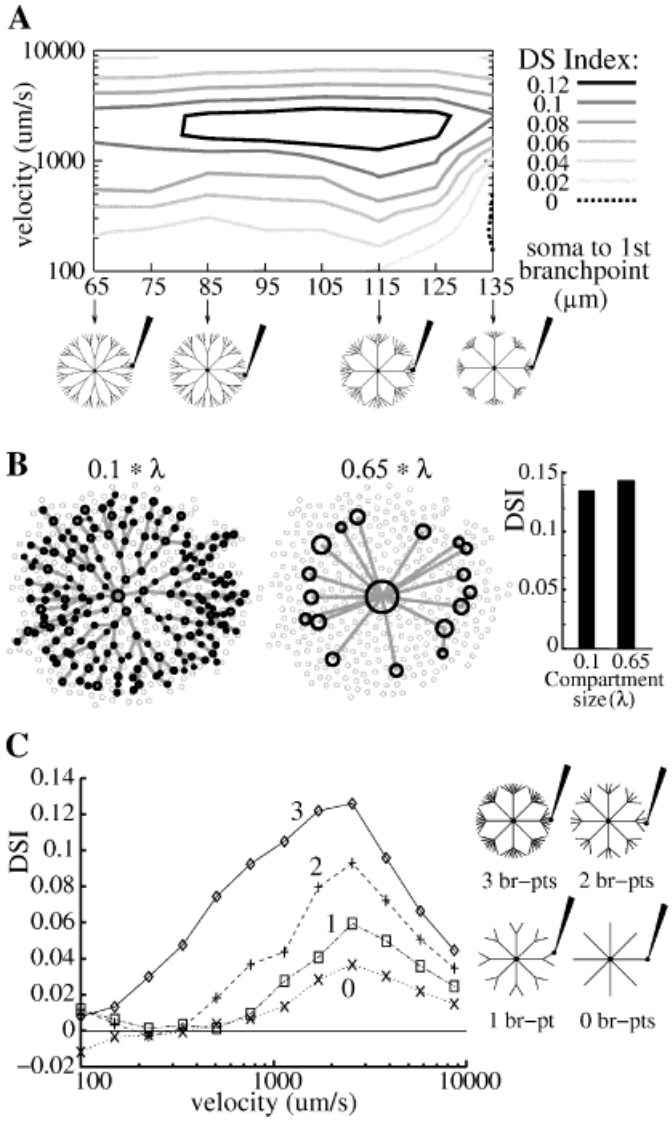

Fig. 6. DS is influenced more by strength of synaptic input than by exact branching pattern. Bar stimuli. A: More realistic distributed branching did not improve DS over limited, "brush-like", distal branching. Artificially generated cells were created with the first branch-point at different radial distances from the soma (abscissa of graph), while dendritic tips remained at same position. Each morphology collected different numbers of synaptic inputs proportional to area covered. For these morphologies bar stimuli elicited responses with similar *DSI* values. When the first branch-point was distal (135 μm), the model cells had fewer distal inputs and a lower *DSI*. Distance to first branch-point was varied in steps of 10 μm. Four of the morphologies are illustrated below. B: Details of morphology do not affect DS. Morphology of real cell (sbac3) portrayed as compartments generated internally by the simulator (dark circles), modeled at fine (0.1 λ) and coarse (0.65 λ) spatial resolution (see *Methods*). Lines between the compartments represent the axial resistances. The pattern of inputs from the array of bipolar cells (small light circles) was kept intact. Both models gave similar DS results. C: Number of distal inputs is important for DS. Morphology varied from 0 to 3 branch-points to change the branching density and thus the number of distal inputs (*right*). To maximize the electrotonic distance from the dendritic tips to the soma, all branching was limited to the outer 20% of the dendritic tree. The cell with three branch-points, and thus the largest density of branching, showed the highest *DSI*.

cells. At extreme *Ri* values, all points would reflect either the local input (large *Ri*) or the global input (small *Ri*). This result suggested that DS requires a balance of local and global inputs.

Simulations using sine-wave stimuli

To measure the sensitivity of the DS generating mechanism to different spatial and temporal frequencies, we performed a series of simulations with drifting sine-wave gratings. The amount of DS at the dendritic tips generated in response to drifting sine waves depended strongly on the spatial frequency and the velocity. The centripetal response was attenuated at high velocities while the centrifugal response was relatively unaffected by velocity (Figs. 8A & 8B). Consistent with this, *DSI* increased with velocity up to a maximum *DSI* of 0.9. The strength of this velocity tuning was strongly affected by the spatial frequency: at some spatial frequencies *DSI* was almost zero and unaffected by velocity (Fig. 9A), but at other spatial frequencies, *DSI* varied broadly with velocity, similar to the velocity tuning shown by bar stimuli. The largest *DSI* occurred above 2000 μm/s for 0.5 cycles/radius. For spatial frequencies that gave robust *DSI* at the dendritic tip, the orientation tuning was approximately proportional to the cosine of the direction of motion relative to the dendrite, that is, maximal for movement parallel to the dendrite (not illustrated). For spatial frequencies that gave weak DS at the dendritic tip, the orientation tuning was much broader or nonexistent. Sine-wave gratings produced almost no DS at the somas of the starburst cells (not illustrated).

Responses to sine-wave annuli

To allow comparison with previous work, we included "bull's eye" stimuli consisting of contracting and expanding concentric sine-wave annuli centered on the soma (Euler et al., 2002). Since DS at the soma of a real starburst cell had been measured with a mask over the proximal part of its dendritic tree (Euler et al., 2002), we also ran simulations with a circular mask covering the most proximal 30% of the dendrites.

The *DSI* elicited in our simulations by sine-wave annuli was strongly dependent on velocity, spatial frequency, and the presence of the mask, giving clear maxima for some combinations of these

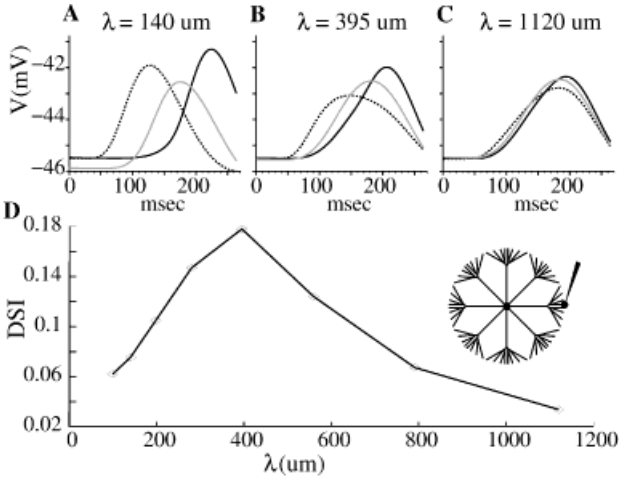

Fig. 7. DS depends on partial summation of local and global inputs. A: A high degree of isolation (small λ) gives a small difference in the peak responses for the two directions (dark traces). B: When dendritic tips are partially isolated, current flows farther along the dendrite, allowing global EPSPs to sum with the local EPSPs, producing greater DS. C: With very little electrotonic isolation, current spreads efficiently throughout the cell so that all EPSPs are essentially identical. D: Effect of electrotonic length constant, using the same morphology as in Fig. 6C, with three branch-points all located distally. The length constant was set by varying axial resistance R_i. Bar stimulus; velocity $\sim$ 2600 μm/s.

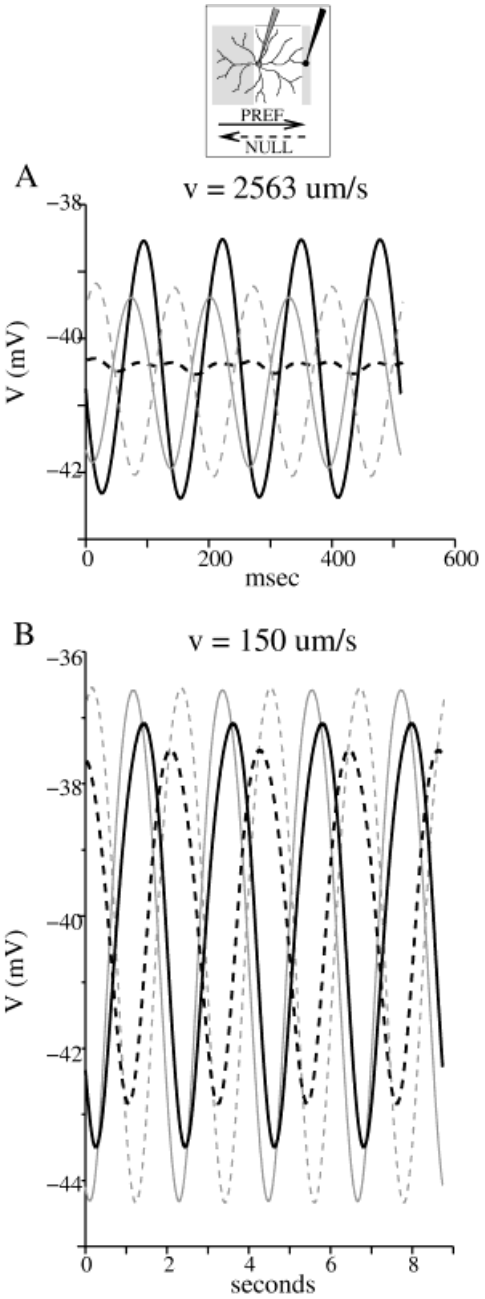

Fig. 8. DS for sine-wave gratings can be nearly maximal (*DSI* $\sim$1), but depends on velocity. Continuous traces, centrifugal motion; dashed traces, centripetal motion. A: High velocity. Dendritic tip shows robust DS (dark traces, *DSI* = 0.9), while the soma shows weak negative DS (light traces, *DSI* = $-$0.04). The null trace (dark dashed trace) is not a pure sinusoid, showing some higher harmonic content generated by slight synaptic nonlinearity. B: Low velocity. The same dendritic tip shows weak DS (dark traces; *DSI* = 0.06) and the soma shows none. Stimulus grating period, 0.5 cycles per radius (328 μm). Cell sb1.

parameters. Responses at the dendritic tips to sine-wave annuli without the mask gave two distinct *DSI* peaks, with an intermediate region of zero or even negative DS (Fig. 9B). Interestingly, the opposite pattern occurred when *DSI* was computed at the soma: two distinct troughs of negative *DSI* with an intermediate region of positive *DSI* (Fig. 9C). The strong anticorrelation between somatic and dendritic *DSI* indicated that both sites are involved in generating DS. At 0.5 cycles/radius this stimulus resembled the "annulus" stimulus used in the earlier simulations (Fig. 5C), both cases producing weak DS (*DSI* $<$ 0.05).

Masking the central region of the dendritic tree broadened the range of positive *DSI* at lower spatial frequencies and shifted the negative *DSI* trough towards higher spatial frequencies (Figs. 9D & 9E). The mask shifted the range of spatial frequencies that elicited robust *DSI* to about 2 cycles/radius, with a peak at around 1.5 cycles/radius. At higher spatial frequencies (2–2.5 cycles/radius) there was again an area of zero or negative *DSI*, and at the highest frequencies *DSI* was positive again. The opposite of this pattern was found at the soma (Fig. 9E).

To understand why sine-wave annuli and gratings gave different DS responses, we generated roughly symmetric, realistic-looking artificial morphologies (Fig. 10A) so that we could evaluate which factors of morphology could account for this difference. When we measured the DS responses of these cells to bars and sine-wave gratings, we found them to be almost identical (not illustrated) to those generated with real morphologies (Figs. 5A & 9). However, the responses to sine-wave annuli with this morphology contained almost no DS (Fig. 10C, Left). The amount of DS did not increase when we varied branching angles and distances, somatic and dendritic diameters, or distributions of varicosities (not illustrated). We hypothesized that a sine-wave annulus elicits less DS in such a symmetrical cell because the annulus gives simultaneous inputs to all points at a given radius, thus preventing effective interaction of signals from different parts of the cell. To test this hypothesis, we reduced the number of dendritic tips that would receive simultaneous inputs, by generating a cell with a randomized total dendritic length (Fig. 10B). Such reduced symmetry gave higher *DSI* values for sine-wave annuli, comparable to *DSI* from the real morphologies for sine-wave annuli (Fig. 10C Right), supporting the hypothesis.

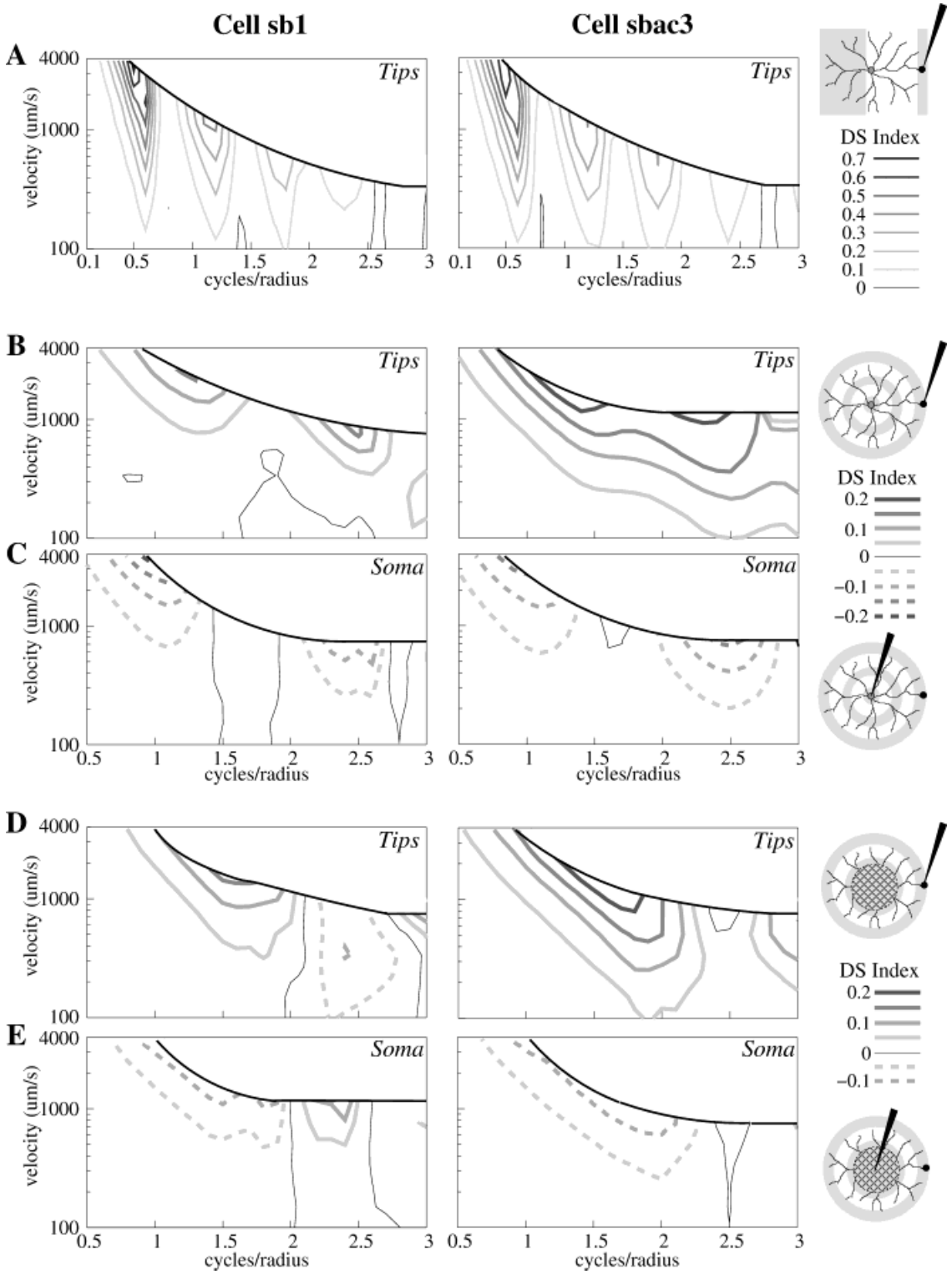

Fig. 9. DS in response to sine-wave stimuli strongly depends on velocity and spatial period. Contour plots show DS as a function of spatial frequency and velocity. A: Sine-wave grating; recording from dendritic tips. *DSI* increases with velocity, peaking at regular intervals in spatial period, near maximal at 0.5 cycles/radius. At the soma, $DSI<0.1$ (not illustrated). Stimulus motion at dendritic tip was always radial. B: Sine wave annulus; recording from dendritic tips, two positive *DSI* peaks (~1 and ~2.5 cycles/radius). C: Sine-wave annulus; recording from soma, two negative *DSI* peaks that correspond to positive peaks found at dendritic tips. D: Sine-wave annulus with gray center mask; recording from dendritic tips, one broad positive peak and smaller negative peak. E: Sine-wave annulus with gray center mask; recording from soma, one broad negative peak and smaller positive peak, corresponding inversely to peaks found at dendritic tips. Plots show average *DSI* for 16 dendritic orientations; the blank region at the top right of each panel, bounded by the thick black line, gave subthreshold responses. Cycles/radius denotes spatial frequency per dendritic length.

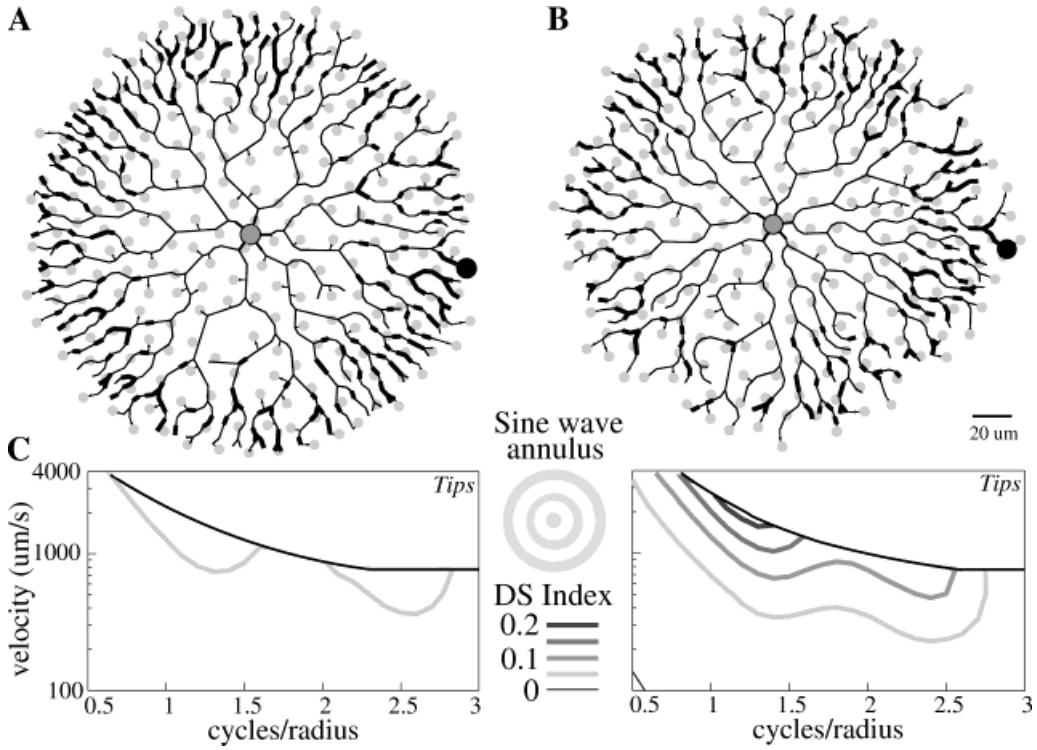

Fig. 10. DS for sine-wave annuli depends on variation in dendritic length. Artificially generated cells with constant (A) and varying (B) dendritic length differ in their responses to sine-wave annuli. C: The average *DSI* at the dendritic tips is ~3-fold greater for a cell with variable dendritic length than for a more symmetric cell. Responses to sine-wave gratings were similar for both (not illustrated). Morphology was created by an algorithm that generated dendritic stubs emanating from the soma, endowed them with the properties of mutual avoidance and tendency for branching, and extended them to a specified dendritic tree radius (see *Methods*). Varicosities were added randomly at the distal dendrites.

Simple summation model

Since our computational model linearly summed signals from many different points, we designed a simpler mathematical summation model to provide intuition about how DS was generated (Fig. 11). The mathematical model consisted of a summation of two sine-wave signals representing local synaptic input at a dendritic tip and at the soma.

Using the simulator with real morphology, we recorded the voltage responses at a dendritic tip and measured the relative attenuation and phase delay between identical temporal sine waves presented separately at either the dendritic tip or the soma. The signal elicited by the somatic stimulus was attenuated and phase delayed relative to the signal elicited by the dendritic tip stimulus (Fig. 11A). A particular combination of velocity and spatial frequency set the temporal frequency. Having determined the relative phase and amplitude of responses at the dendritic tip, we introduced a time delay to simulate a grating moving towards or away from the soma. To simulate centripetal motion, we added a time delay to the soma signal (NULL direction, Fig. 11B). Next, we summed the signals elicited by the two stimuli (tip, delayed soma) to produce the dendritic tip response. To simulate centrifugal motion, we added a time delay to the dendritic tip signal (PREF direction, Fig. 11C) and again summed the signals (delayed tip, soma) to produce a dendritic tip response. DS is evident in the different summed response amplitudes for the two directions. The reason was that the phase delay from the signal traveling in the *dendrite* from soma to tip remained constant with direction, while the phase delay from the *stimulus* changed with direction. The two delays (*dendrite*, *stimulus*) tended to cancel or reinforce depending on the direction, generating a large or small sine wave.

Not surprisingly the simple mathematical model produced a strong and systematic dependence of DS on velocity and spatial frequency (Fig. 11D). The pattern of *DSI* consisted of alternating positive and negative lobes at specific spatial frequencies, peaking at velocities corresponding to about 7 Hz. No DS occurred at intermediate spatial frequencies, where the stimulus-dependent time delay was a multiple of a half cycle, which gave equal sums for both directions. These results were qualitatively similar to the simulation results for sine-wave stimuli in the full model (Fig. 9; see also Discussion).

Calcium channels

To explore how much DS would be generated at the synaptic output, given the DS responses generated in our models, we added voltage-dependent calcium channels at the outer third of the dendritic tree. We chose Q-type channels because they exist in starburst cells (Cohen, 2001) and blocking them pharmacologically abolishes DS in the DSGC (Jensen, 1995), suggesting that Q-type channels are associated with the starburst's synaptic output.

The Q-type calcium channels in the model had a voltage threshold at about −40 mV and a sharply nonlinear *I–V* curve (Fig. 2B; Sather et al., 1993). We measured the $[Ca^{2+}]_i$ at the dendritic tip in response to a bar moving to and fro across the cell

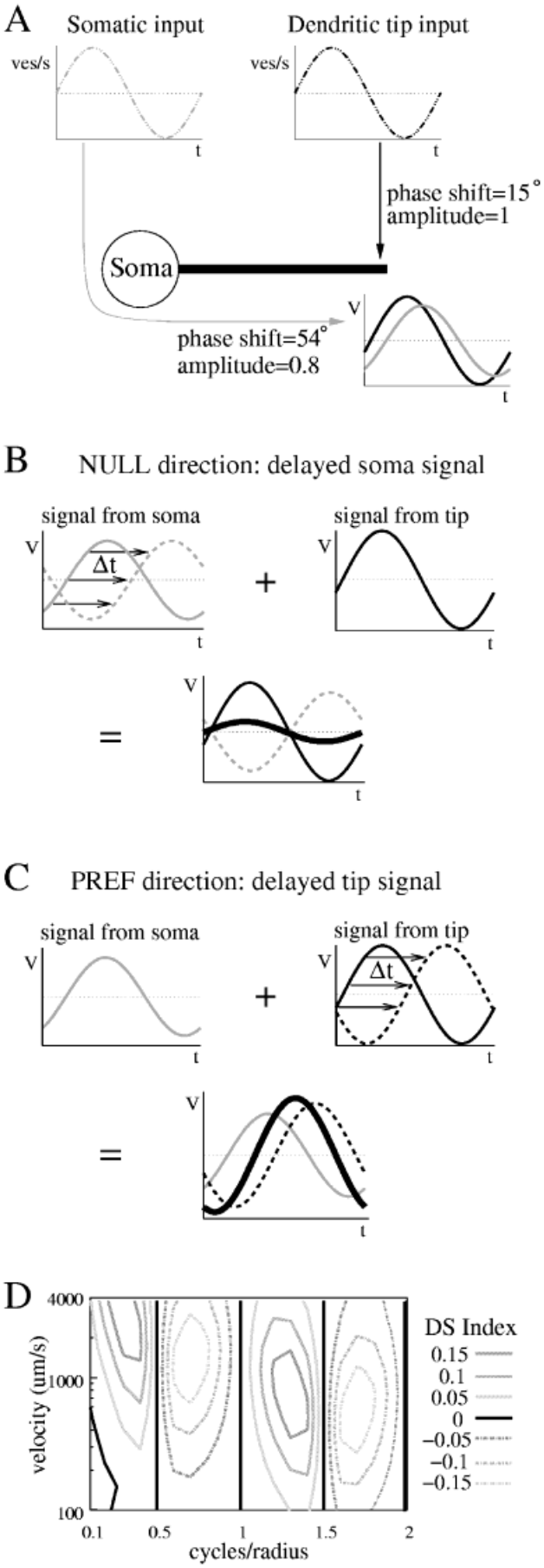

Fig. 11. Simple mathematical model produces DS by linear summation of two sine waves at the dendritic tip. Their temporal frequency was set by a particular combination of velocity and spatial frequency (7 Hz shown). A: Using the simulator, we measured the relative amplitude and phase of voltage responses at the dendritic tip to identical temporal sine-wave stimuli presented separately to single synaptic inputs at the soma (gray trace) and dendritic tip (dashed trace). B: Null direction: the sine wave resulting from somatic stimulation (light trace) is delayed by Δt (light dashed trace) to simulate centripetal motion. Adding this delayed signal to the signal resulting from the tip stimulation (dark trace) produces a sine wave of small amplitude (thick dark trace). C: Preferred direction: the sine wave resulting from the tip stimulation (dark trace) is delayed (dark dashed trace) to simulate centrifugal motion. Adding this delayed tip signal to the signal resulting from the somatic stimulation (light trace) produces a sine wave of large amplitude (thick dark trace). D: Computing the temporal frequency and phase delay for a range of velocities and spatial frequencies, we summed signals resulting from soma and tip stimulation as described above, and found DS comparable to the simulation results from real morphologies (Fig. 9A) with peaks occurring at regular intervals in spatial period. The negative peaks resulted from the fact that only two inputs were included (see *Discussion*).

and quantified the directionality by computing a *DSI* based on the peak level of $[Ca^{2+}]_i$ denoted here by DSCa (Fig. 12). The values of DSCa depend on the *DSI* values in the voltage responses and on the amplitude of the voltage responses. For robust DS, the response for the preferred direction must be sufficiently larger ("above threshold") than the response in the null direction ("below threshold"). To achieve this, we set the cone synaptic properties (signal gain, offset) to give responses in the optimal voltage range. At the optimal stimulus speeds (~1000 μm/s), the DSCa at the dendritic tips was up to 3-fold larger than the *DSI* of the voltage signal (Fig. 12), suggesting that calcium channels could serve to amplify the DS in the voltage responses of starburst cells. The effects of calcium channels are velocity dependent because the size of the voltage responses also depends on velocity. The amplitude of responses in real starburst dendrites is not known, but it seems reasonable to assume feedback mechanisms could keep the responses in the correct range.

Discussion

Our results show for a variety of stimuli that the morphology of the starburst cell, with only excitatory synaptic input and passive membrane properties, can generate direction selectivity at its dendritic tips where the synaptic outputs are located (Famiglietti, 1991). The amount of DS depended strongly on the type of stimulus. Bar stimuli gave a DS index of up to 0.2, and sine-wave stimuli gave a DS index of up to 0.9. The optimal stimulus for generating DS was a sine-wave grating with large spatial period (~400 μm, twice the dendritic length) moving at high velocities (~5000 μm/s). Further, our results show that the addition of voltage-gated calcium channels can amplify a difference in the response wave-shape produced by morphological properties. These results extend previous models of DS in the starburst amacrine cell (Borg-Graham & Grzywacz, 1992; Poznanski, 1992).

Mechanism for DS

DS in our model depended on the summation of local and global signals, which differed depending on the direction of the stimulus

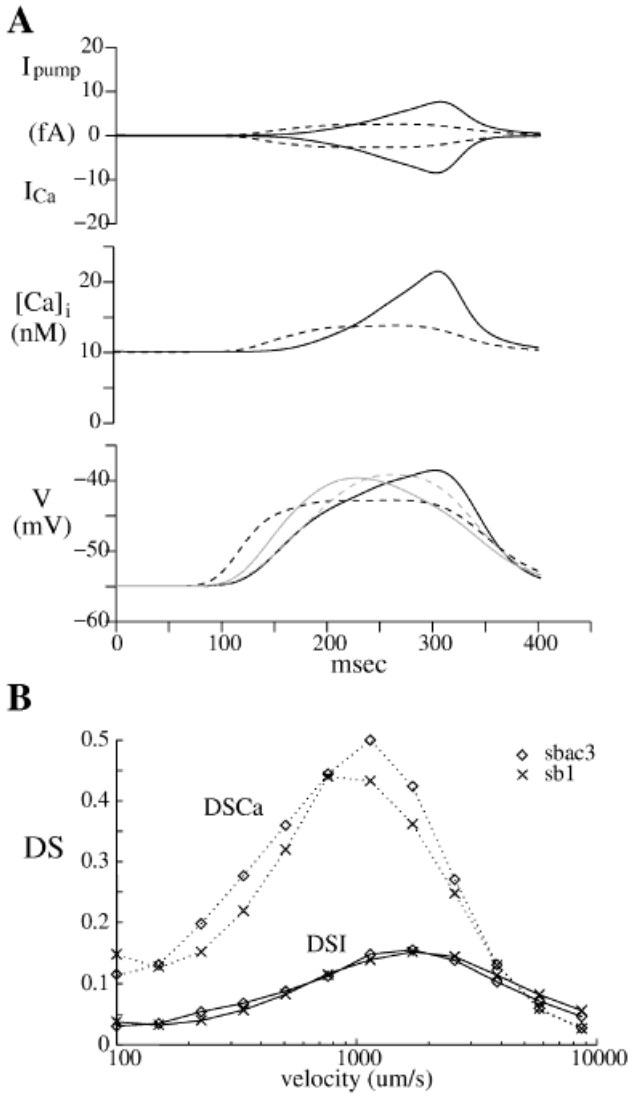

Fig. 12. Calcium channel nonlinearity amplifies the DS response. A: Top: Calcium enters the cell *via* calcium channels (I_{Ca}) and is pumped out by calcium pumps (I_{pump}). Middle: peak $[Ca^{2+}]_i$ is greater in response to the preferred direction. Bottom: voltage traces for the two directions superimposed in the same graph. Dashed lines, null; continuous lines, preferred. Cell sb1; bar stimulus; velocity = 2000 μm/s. B: DS in the $[Ca^{2+}]_i$ signal ("DSCa") is significantly higher that the *DSI* in the voltage signal. For these simulations, we adjusted the synaptic gains and offsets to produce responses within the working range of the calcium channels.

(Fig. 4). For centrifugal motion of a bar, both local and global signals reach their peak as the bar passes over the dendritic tips, and therefore they temporally sum. For centripetal motion the local and global signals sum less effectively because the local and global peaks do not coincide. This mechanism depends on two factors derived from the starburst morphology. First, partial electrotonic isolation of the dendritic tips from the soma (and the rest of the cell) allows separate local and global signals to interact and causes a higher input resistance at the dendritic tips, amplifying the local signal (Velte & Miller, 1997). Second, the number of inputs collected at the distal zones of a dendrite is predicted to be greater than at the proximal zones. This prediction follows from the wedge-shaped dendritic spread, with more membrane surface area in the distal than the proximal portion, and from the assumption that the number of inputs per unit length of dendrite is uniform across the dendritic tree (see Fig. 1; Methods; Freed & Sterling, 1988; Cohen & Sterling, 1990; Kier et al., 1995). Both the number of distal inputs and the degree of electrotonic coupling are influenced by the extensive branching at the distal zone, and are therefore interrelated. The specific values we found for *DSI* and velocity depend on the parameters we chose for the simulation, but since the model was linear, this mechanism of DS is independent of any particular choice of parameters.

The ability of the starburst morphology to generate DS depends on the length constant λ (Fig. 7; Rall, 1964, 1967; Poznanski, 1992; Borg-Graham & Grzywacz, 1992). A large length constant implies that inputs are not localized because there is little attenuation of current as it spreads through the cell. In this case, the recorded signal mostly reflects the global input pattern. Since the starburst morphology is symmetric, this global input pattern is isotropic. A small length constant attenuates the global signal at the dendritic tip relative to the local signal (Rall, 1959; Miller & Bloomfield, 1983; Poznanski, 1992; Velte & Miller, 1997). However, since the local synaptic input is also isotropic, it cannot independently create DS. Therefore to generate an asymmetry such as DS requires an intermediate degree of electrotonic coupling (Fig. 7). The optimal length constant ($\sim$400 μm in our model) allows current to spread throughout the cell to contribute to signals at the dendritic tips, but attenuates this current enough that it does not generate identical signals at all points (Euler et al., 2002). This is inconsistent with each dendrite forming an independent computational unit (Miller & Bloomfield, 1983) because the global signal from the soma is a necessary component of this DS mechanism.

A simple annulus is not an effective stimulus for generating DS because it produces symmetric activation of every dendrite simultaneously. With equal activation, equal current flows from the dendrites to the soma, reducing its loading effect, effectively isolating the dendrites (Velte & Miller, 1997). The result is that the signal at the dendritic tips mostly reflects the local synaptic input, which is isotropic. The weak response to symmetrical activation is also evident from our results with a symmetric, artificial morphology stimulated by sine-wave annuli (Fig. 10). In this case, DS was increased by either reducing the symmetry in the cell (Fig. 10B) or using nonsymmetric stimuli (sine waves, bars), implying that DS requires the signals from different dendrites to be out of phase. The fact that DS is not generated optimally in isolated dendrites highlights the global nature of the interactions that generate DS. However, the presence of DS responses with two-spot stimuli indicates that the mechanism can generate DS quite locally.

For sine-wave gratings, the mechanism for DS depends on the interaction between the stimulus-generated time delay and the attenuation and phase lag caused by the cell's electrotonic properties. The phase interactions depend on spatial frequency and velocity. For lower velocities, the time for one stimulus cycle to pass along the length of a dendrite is longer relative to the travel time for a signal through a dendrite. For higher velocities, the temporal period of the stimulus is short and more closely matched to the travel time from soma to tip, allowing the signals to interact, being more in phase or counterphase depending on direction and morphology.

For sine-wave annuli, the mechanism for DS can be reduced to an interaction between signals in the soma and one narrowly branching dendrite because all dendrites are activated synchronously. The DS generated in this case is weak (Fig. 9) compared with DS from sine-wave gratings because for symmetrical stimuli

(as described above) the dendritic signals interact only weakly through the soma. The DS measured for sine-wave annuli at the soma and dendritic tip tend to be opposite in sign (Fig. 9) because, for stimuli that produce DS at the tip, linearity requires the opposite response at the soma. For example, a large response at the dendritic tip to centrifugal motion and a weak response to centripetal motion produce strong DS. But since the system is linear, the signals at soma and tip must sum for both directions to the same total, so that a large response at the tip to centrifugal motion tends to be accompanied by a small response at the soma, and *vice versa*. This analysis applies to results for a simple model containing soma and one dendrite (not illustrated) as well as for symmetrical stimuli where the SBAC morphology reduces to the same case (Fig. 9). It does not apply to a sine-wave grating because a grating, lacking rotational symmetry, creates different patterns of input across each dendrite.

Our results suggest that velocity, spatial frequency, and the presence of a central mask can greatly affect the amount of DS generated depending on the exact combination of parameters. For example, Euler et al. (2002) reported no systematic DS at the soma in response to sine-wave annuli, but found that adding a central mask caused a small but significant increase in DS at the soma. Our results also predict that adding a central mask could increase *DSI* at the soma. However, this would depend on the stimulus spatial frequency: for some spatial frequencies a mask could actually reverse the *DSI* (1.5–2 cycles/radius; see Figs. 9C,E).

A simple mathematical model based on summation of appropriately phase-shifted and attenuated sine waves showed that phase interactions can cause DS (Fig. 11). Not surprisingly, there were some differences between the results generated by this simple mathematical model and those obtained with sine-wave gratings presented to the full morphological model (Fig. 9A), such as the presence of negative DS peaks and sharply demarcated zero DS lines. The difference is explained by interactions among the large number of synaptic inputs summed by the complex dendritic tree. In the full model, the soma collected signals from more synaptic inputs, giving a larger global EPSP at the soma than the simple mathematical model. This larger soma signal biased the EPSPs from Preferred and Null directions towards positive DS at the dendritic tips. We checked this by presenting sine-wave gratings to a branchless single dendrite model. Although this model differed from the mathematical model in receiving synaptic inputs along the length of the dendrite, it was similar in having soma and only one dendrite. The pattern of its DS also had both positive and negative lobes (not illustrated), similar to the simple mathematical model, implying that the difference between DS of full and single dendrite models originated in the remainder of the dendritic tree. Given the simplicity of the mathematical model, the results seemed remarkably consistent with our computational model results (Figs. 9A & 11D). In both, there is a clear dependence on spatial frequency with specific *DSI* peaks and an absence of DS at intermediate frequencies.

We found that DS generated by sine-wave gratings was often greater than for bars. While thin bars gave more DS than wide bars, wide sine waves (having the largest spatial period) gave the greatest DS. The salient difference is that the positive and negative half-cycles of sine waves can cancel when superimposed, but this cannot happen with bars or other nonperiodic stimuli in the absence of inhibition. This suggests that a model including appropriate inhibition could amplify DS generated by morphology.

Although some evidence suggests a role for inhibition in generating DS in the SBAC (Borg-Graham & Grzywacz, 1992; Brandstätter et al., 1995; Gavrikov et al., 2003), our study explicitly did not include inhibition in order to evaluate the role of morphology. Our results do not preclude a role for inhibition, but show that to generate DS it is not necessary. A recent extracellular study showed that the directionality of spiking in the SBAC was reduced in the presence of a $GABA_C$ blocker (Gavrikov et al., 2003). This is not inconsistent with our model because it did not include regenerative membrane properties.

Nonlinear amplification of DS signal

DS has classically been defined by a difference in the time integrals of the responses, requiring a nonlinearity (Hassenstein & Reichardt, 1956). This role might be fulfilled by interactions between inhibitory and excitatory inputs (Torre & Poggio, 1978; Borg-Graham & Grzywacz, 1992; Gavrikov et al., 2003). However, since DS measured in the calcium signal from starburst dendrites is unaffected by GABA blockers (Euler et al., 2002; T. Euler, personal communication), we investigated the effect of a nonlinearity resulting from the activity of voltage-gated calcium channels. Our simulations showed that calcium channels could effectively provide a threshold, which amplified DS ~2–4 fold (Fig. 12).

Since blocking Q-type calcium channels removes DS from the DS ganglion cell (Jensen, 1995), and evidence exists that Q-type channels are actually present in the starburst (Cohen, 2001), the inclusion of Q-type channels in our model represents a plausible hypothesis about the localization, kinetics, and conductance of these channels (Fig. 2). However, it is not known whether voltage in the starburst cell is a linear function of its synaptic inputs, as in our model. For example, Ca^{2+} or Na^{+} channels might provide regenerative currents that modify the processing inside adult starburst dendrites (Taylor & Wässle, 1995; Bloomfield, 1996; Peters & Masland, 1996; Zhou & Fain, 1996; Velte and Miller, 1997; T. Euler, personal communication). Our simulations with calcium channels obviated any such regenerative effect by setting a very low channel density, so that the enhancement of the DS signal resulted entirely from nonlinear activation of the channels (Fig. 12). Higher calcium channel densities that would allow some regenerative depolarization might produce even more enhancement. However, since such an effect has not been shown in the SBAC, our results provide a plausible mechanism for the finding by Euler et al. (2002) of a direction-selective $[Ca^{2+}]_i$ signal in tips of stimulated dendrites.

Synaptic outputs

The starburst amacrine is known to release ACh and GABA (Brecha et al., 1988; Vaney & Young, 1988; O'Malley & Masland, 1989). Since this release is thought to be nonlinearly dependent on voltage (Schwartz, 1987; O'Malley et al., 1992), our simulations showing nonlinear activation of calcium channels suggest how much DS synaptic outputs might convey (Fig. 12). A sharp threshold would require a mechanism of adaptation to keep the evoked voltage responses in the starburst within a limited range, especially if they are small. Such adaptation is a well-known attribute of retinal neurons of the inner plexiform layer. For example, bipolar cells are known to have nonlinear release of neurotransmitter that is closely regulated by feedback (Tachibana & Kaneko, 1988; Mao et al., 2002; Shields & Lukasiewicz, 2003).

For a mechanism of DS based on processing within the starburst dendrites to function correctly, a starburst amacrine cell must

make specific connections from the outer third of its dendritic tree to DS ganglion cells, based on the orientation of its dendrites (Vaney et al., 1989; Famiglietti, 1991; Fried et al., 2002; but see Famiglietti, 2002). Such a DS signal coded in transmitter release from starburst cells could provide the ganglion cells' direction-selective input (Euler et al., 2002; Fried et al., 2002; Taylor & Vaney, 2002).

The starburst cell's simulated responses to stimuli at different orientations showed a large variability in the amount of *DSI* between dendrites (Fig. 5A), consistent with previous work (Euler et al., 2002). This suggests that, for any single stimulus orientation, the response of one dendrite would not be reliable so that pooling of responses from dendrites with similar orientations (from other SBACs) would be required to provide a reliable signal to the DSGC. Although the high degree of overlap of starburst cells in the retina (a coverage factor of up to 70; Vaney, 1984) would seem to be consistent with this prediction, the number of starburst cells needed to effectively provide directional signals to DSGCs is unknown. Therefore it would be helpful to look in more detail at the interactions between a number of starburst cells and a DSGC. Alternatively, the local circuit around each dendrite may provide a more robust *DSI* signal to the DSGC through synaptic connections with neighboring starburst cells, bipolar cells, and other types of amacrine cells (Millar & Morgan, 1987; Mariani & Hersh, 1988; Dacheux et al., 2003; Yamada et al., 2003).

Acknowledgments

We thank T. Euler and S. Hausselt for reading the manuscript, and F. Amthor, H. Barlow, L. Borg-Graham, W. Denk, S. Fried, T. Münch, K.-P. Hoffmann, and P. Sterling for helpful comments. This research was supported by MH48168 to R.G. Smith, and NHMRC179837 and EY014888 to W.R. Taylor.

References

Amthor, F.R., Keyser, K.T. & Dmitrieva, N.A. (2002). Effects of the destruction of starburst-cholinergic amacrine cells by the toxin AF64A on rabbit retinal directional selectivity. *Visual Neuroscience* **19**, 495–509.

Barlow, H.B. & Hill, R.M. (1963). Selective sensitivity to direction of movement in ganglion cells of the rabbit retina. *Science* **139**, 412–414.

Bloomfield, S.A. (1996). Effect of spike blockade on the receptive-field size of amacrine and ganglion cells in the rabbit. *Journal of Neurophysiology* **75**, 1878–1893.

Borg-Graham, L.J. & Grzywacz, N.M. (1992). A model of the directional selectivity circuit in retina: Transformations by neurons singly and in concert. In *Single Neuron Computation*, ed. McKenna, T., Davis, J. & Zornetzer, S.F., pp. 347–376. New York: Academic Press, Inc.

Brandstätter, J.H., Greferath, U., Euler, T. & Wässle, H. (1995). Co-stratification of $GABA_A$ receptors with the directionally selective circuitry of the rat retina. *Visual Neuroscience* **12**, 345–358.

Brecha, N., Johnson, D., Peichl, L. & Wässle, H. (1988). Cholinergic amacrine cells of the rabbit retina contain glutamate decarboxylase and γ-aminobutyrate immunoreactivity. *Proceedings of the National Academy of Sciences of the U.S.A.* **85**, 6187–6191.

Cohen, E. (2001). Voltage-gated calcium and sodium currents of starburst amacrine cells in the rabbit retina. *Visual Neuroscience* **18**, 799–809.

Cohen, E. & Sterling, P. (1990). Demonstration of cell types among cone bipolar neurons of cat retina. *Philosophical Transactions of the Royal Society B* (London) **330**, 305–321.

Dacheux, R.F., Chimento, M.F. & Amthor, F.R. (2003). Synaptic input to the On–Off directionally selective ganglion cell in the rabbit retina. *Journal of Comparative Neurology* **456**, 267–278.

Euler, T., Detwiler, P.B. & Denk, W. (2002). Directionally selective calcium signals in dendrites of starburst amacrine cells. *Nature* **418**, 845–852.

Famiglietti, E.V. (1983). On and off pathways through amacrine cells in mammalian retina: The synaptic connections of "starburst" amacrine cells. *Vision Research* **23**, 1265–1279.

Famiglietti, E.V. (1991). Synaptic organization of starburst amacrine cells in rabbit retina: Analysis of serial thin sections by electron microscopy and graphic reconstruction. *Journal of Comparative Neurology* **309**, 40–70.

Famiglietti, E.V. (2002). A structural basis for omnidirectional connections between starburst amacrine cells and directionally selective ganglion cells in rabbit retina, with associated bipolar cells. *Visual Neuroscience* **19**, 145–162.

Freed, M.A. & Sterling, P. (1988). The ON-alpha ganglion cell of the cat retina and its presynaptic cell types. *Journal of Neuroscience* **8**, 2303–2320.

Fried, S.I., Münch, T.A. & Werblin, F.S. (2002). Mechanisms and circuitry underlying directional selectivity in the retina. *Nature* **420**, 411–414.

Gavrikov, K.E., Dmitriev, A.V., Keyser, K.T. & Mangel, S.C. (2003) Cation-chloride cotransporters mediate neural computation in the retina. *Proceedings of the National Academy of Sciences of the U.S.A.* **100**, 16047–16052.

Hassenstein, B. & Reichardt, W.E. (1956). Functional structure of a mechanism of perception of optical movement. *Proceedings 1st International Congress Cybernetics Namar*, 797–801.

He, S. & Masland, R.H. (1997). Retinal direction selectivity after targeted laser ablation of starburst amacrine cells. *Nature* **389**, 378–382.

Jensen, R.J. (1995). Effects of Ca^{2+} channel blockers on directional selectivity of rabbit retinal ganglion cells. *Journal of Neurophysiology* **74**, 12–23.

Joyner, R.W., Westerfield, M., Moore, J.W. & Stockbridge, N. (1978). A numerical method to model excitable cells. *Biophysical Journal* **22**, 155–170.

Kier, C.K., Buchsbaum, G. & Sterling, P. (1995). How retinal microcircuits scale for ganglion cells of different size. *Journal of Neuroscience* **15**, 7673–7683.

Mao, B.Q., MacLeish, P.R. & Victor, J.D. (2002). Relation between potassium-channel kinetics and the intrinsic dynamics in isolated retinal bipolar cells. *Journal of Computational Neuroscience* **12**, 147–163.

Mariani, A.P. & Hersh, L.B. (1988). Synaptic organization of cholinergic amacrine cells in the rhesus monkey retina. *Journal of Comparative Neurology* **267**, 269–280.

Maturana, H.R., Lettvin, J.Y., McCulloch, W.S. & Pitts, W.H. (1960). Anatomy and physiology of vision in the frog (*rana pipiens*). *Journal of General Physiology* **43** (Suppl. 2), 129–171.

Millar, T.J. & Morgan, I.G. (1987). Cholinergic amacrine cells in the rabbit retina synapse onto other cholinergic amacrine cells. *Neuroscience Letters* **74**, 281–285.

Miller, R.F. & Bloomfield, S.A (1983). Electroanatomy of a unique amacrine cell in the rabbit retina. *Proceedings of the National Academy of Sciences of the U.S.A.* **80**, 3069–3073.

O'Malley, D.M. & Masland, R.H. (1989). Co-release of acetylcholine and γ-aminobutyric acid by a retinal neuron. *Proceedings of the National Academy of Sciences of the U.S.A.* **85**, 6187–6191.

O'Malley, D.M., Sandell, J.H. & Masland, R.H. (1992). Co-release of acetylcholine and GABA by the starburst amacrine cells. *Journal of Neuroscience* **12**, 1394–1408.

Perkel, D.H. & Mulloney, B. (1978). Elecrotonic properties of neurons: steady-state compartmental model. *Journal of Neurophysiology* **41**, 621–639.

Peters, B.N. & Masland, R.H. (1996). Responses to light of starburst amacrine cells. *Journal of Neurophysiology* **75**, 469–480.

Poznanski, R.R. (1992). Modelling the electrotonic structure of starburst amacrine cells in the rabbit retina: A functional interpretation of dendritic morphology. *Bulletin of Mathematical Biology* **54**, 905–928.

Rall, W. (1959). Branching dendritic trees and motoneuron membrane resistivity. *Experimental Neurology* **1**, 491–527.

Rall, W. (1964). Theoretical significance of dendritic trees for neuronal input–output relations. In *Neural Theory and Modeling*, ed. Reis, R.F., pp. 72–97. Stanford, California: Stanford University Press.

Rall, W. (1967). Distinguishing theoretical synaptic potentials computed for different soma-dendritic distributions of synaptic input. *Journal of Neurophysiology* **30**, 1138–1168.

Sather, W.A., Tanabe, T., Zhang, J.-F., Mori, Y., Adams, M.E. & Tsien, R.W. (1993). Distinctive biophysical and pharmacological properties of Class A (BI) calcium channel α_1 subunits. *Neuron* **11**, 291–303.

SCHNEEWEIS, D.M. & SCHNAPF, J.L. (1999). The photovoltage of macaque cone photoreceptors: Adaptation, noise, and kinetics. *Journal of Neuroscience* **19**, 1203–1216.

SCHWARTZ, E.A. (1987). Depolarization without calcium can release gamma-aminobutyric acid from a retinal neuron. *Science* **238**, 350–355.

SERRANO, J.R., PEREZ-REYES, E. & JONES, S.W. (1999). State-dependent inactivation of the alpha1G T-type calcium channel. *Journal of General Physiology* **114**, 185–201.

SHIELDS, C.R. & LUKASIEWICZ, P.D. (2003). Spike-dependent GABA inputs to bipolar cell axon terminals contribute to lateral inhibition of retinal ganglion cells. *Journal of Neurophysiology* **89**, 2449–2458.

SMITH, R.G. (1992). NeuronC: A computational language for investigating functional architecture of neural circuits. *Journal of Neuroscience Methods* **43**, 83–108.

SMITH, R.G. (2004). The NeuronC neural circuit simulation language. Available for academic use at: ftp://retina.anatomy.upenn.edu/pub/nc.tgz.

TACHIBANA, M. & KANEKO, A. (1988). Retinal bipolar cells receive negative feedback input from GABAergic amacrine cells. *Visual Neuroscience* **1**, 297–305.

TAUCHI, M. & MASLAND, R.H. (1984). The shape and arrangement of the cholinergic neurons in the rabbit retina. *Proceedings of the Royal Society B* (London) **223**, 101–191.

TAYLOR, W.R. & VANEY, D.I. (2002). Diverse synaptic mechanisms generate direction selectivity in the rabbit retina. *Journal of Neuroscience* **22**, 7712–7720.

TAYLOR, W.R. & WÄSSLE, H. (1995). Receptive field properties of cholinergic amacrine cells in the rabbit retina. *European Journal of Neuroscience* **7**, 2308–2321.

TORRE, V. & POGGIO, T. (1978). A synaptic mechanism possibly underlying directional selectivity to motion. *Proceedings of the Royal Society* (London) **202**, 409–416.

VANEY, D.I. (1984). "Coronate" amacrine cells in the rabbit retina have the "starburst" dendritic morphology. Proceedings of the Royal Society of London Series B. *Biological Sciences* **220**, 501–508.

VANEY, D.I., COLLIN, S.P. & YOUNG, H.M. (1989). Dendritic relationships between cholinergic amacrine cells and direction-selective ganglion cells. In *Neurobiology of the Inner Retina*, ed. Weiler, R. & Osborne, N.N., pp. 157–168. Berlin: Springer.

VANEY, D.I. & YOUNG, H.M. (1988). GABA-like immunoreactivity in cholinergic amacrine cells of the rabbit retina. *Brain Research* **438**, 369–373.

VAN ROSSUM, M.C., O'BRIEN, B.J. & SMITH, R.G. (2003). Effects of noise on the spike timing precision of retinal ganglion cells. *Journal of Neurophysiology* **89**, 2406–2419.

VELTE, T.J. & MILLER, R.F. (1997). Spiking and nonspiking models of starburst amacrine cells in the rabbit retina. *Visual Neuroscience* **14**, 1073–1088.

WÄSSLE, H. & RIEMANN, H.J. (1978). The mosaic of nerve cells in the mammalian retina. *Proceedings of the Royal Society B (London)* **200**, 441–461.

YAMADA, E.S., DMITRIEVA, N., KEYSER, K.T., LINDSTROM, J.M., HERSH, L.B. & MARSHAK, D.W. (2003). Synaptic connections of starburst amacrine cells and localization of acetylcholine receptors in primate retinas. *Journal of Comparative Neurology* **461**, 76–90.

YOSHIDA, K., WATANABE, D., ISHIKANE, H., TACHIBANA, M., PASTAN, I. & NAKANISHI, S. (2001). A key role of starburst amacrine cells in originating retinal directional selectivity and optokinetic eye movement. *Neuron* **30**, 771–780.

ZHOU, Z.J. & FAIN, G.L. (1996). Starburst amacrine cells change from spiking to non-spiking neurons during retinal development. *Proceedings of the National Academy of Sciences of the U.S.A.* **93**, 8057–8062.